Spectrogram analysis of selected tremor signals using short-time Fourier transform and continuous wavelet transform

Thorsten Bartosch ([1]) **and Dieter Seidl** ([2])
([1]) *Lehrstuhl für Nachrichtentechnik I, Universität Erlangen-Nürnberg, Erlangen, Germany*
([2]) *Bundesanstalt für Geowissenschaften und Rohstoffe, Seismologisches Zentralobservatorium Gräfenberg, Erlangen, Germany*

Abstract
Among a variety of spectrogram methods Short-Time Fourier Transform (STFT) and Continuous Wavelet Transform (CWT) were selected to analyse transients in non-stationary tremor signals. Depending on the properties of the tremor signal a more suitable representation of the signal is gained by CWT. Three selected broadband tremor signals from the volcanos Mt. Stromboli, Mt. Semeru and Mt. Pinatubo were analyzed using both methods. The CWT can also be used to extend the definition of coherency into a time-varying coherency spectrogram. An example is given using array data from the volcano Mt. Stromboli.

Key words *spectrogram – wavelet transform – broadband tremor*

1. Introduction

The information content of a physical quantity either is commonly represented as a function of time or as a Fourier spectrum. However a function of time does not show the spectral content of the signal while the Fourier spectrum cannot extract temporal variations of the signal. A time-frequency representation provides a trade-off between both representations. In the following, two approaches to computing a time-frequency representation are compared.

Mailing address: Dr. Thorsten Bartosch, Lehrstuhl für Nachrichtentechnik I, Universität Erlangen-Nürnberg, Cauerstraße 7, D-91058 Erlangen, Germany; e-mail: thorsten@nt.e-technik.uni-erlangen.de

2. STFT and CWT

The STFT is an integral transform of a signal $f(t)$ defined as

$$S_{\omega,\tau}[f(t)] = \int_{-\infty}^{\infty} f(t)w(t-\tau)e^{-j\omega t}\,dt \qquad (2.1)$$

$$= e^{-j\omega\tau}\int f(t)w(t-\tau)e^{-j\omega(t-\tau)}\,dt. \qquad (2.2)$$

Equation (2.1) may be interpreted as a Fourier spectrum of a signal seen through a sliding window $w(t-\tau)$. If a symmetric window $w(t)$ is chosen then τ identifies the center position of the shifted window $w(t-\tau)$. The weighted signal $f(t)\cdot w(t-\tau)$ trends to zero outside a surrounding of τ. Therefore τ indicates the approximate time for which the Fourier spectrum of $f(t)\cdot w(t-\tau)$ is valid. The arrangement of spectras corresponding to a linear grid of τ values yield a STFT spectrogram. Side-lobes, leakage effects and frequency resolution are influenced by a proper choice of the window function. The

time and frequency resolution can be adjusted by modifying the window length t_w. The smallest measurable frequency is determined by the window length $f_{min} = 1/t_w$.

On the other hand, eq. (2.2) can be identified as a convolution. It can therefore be interpreted as an infinite channel filter bank (Nawab and Quatieri, 1988; Vaidyanathan, 1993), see fig. 1. The impulse responses $h_i(t)$ in fig. 1 differ only in a modulation factor $e^{-j\omega t}$. They can be regarded as modulated versions of a low pass impulse response function which is the window function itself. In the frequency domain it is obvious that their transfer functions $\hat{H}_i(\omega)$ have equal bandwidth but shifted center frequencies depending on the modulation factor. By multiplication with $e^{-j\omega t}$ the filtered signal is shifted into its base band (low pass band) which is equivalent to the computation of the envelope.

Thus we can see that the STFT represents a time-frequency analysis with fixed resolution in the time and frequency dimension. In general, it does not seem possible to find a trade-off between time and frequency resolution which is well-adapted to tremor signals from volcanoes in their entire frequency range. Later on in the text the CWT will be introduced which transforms a signal into a so called time-scale plane (scalogram) thus offering a more suitable trade-off.

The CWT is defined as

$$W_{a,\tau}[f(t)] = \frac{1}{\sqrt{a}} \int_{-\infty}^{\infty} f(t) \Psi^* \left(\frac{t-\tau}{\alpha} \right) dt \quad (2.3)$$

where $\Psi(t)$ is called a wavelet function when it fulfils the admissibility condition

$$0 < \int \frac{\left| \hat{\Psi}(\omega) \right|^2}{|\omega|} d\omega < \infty. \quad (2.4)$$

Where

$$\hat{\Psi}(\omega) = \int_{-\infty}^{\infty} \Psi(t) e^{-j\omega t} dt \quad (2.5)$$

is the definition of the Fourier transform and Ψ^* is the conjugate complex of Ψ. For a detailed representation of the CWT see Daubechies, (1992).

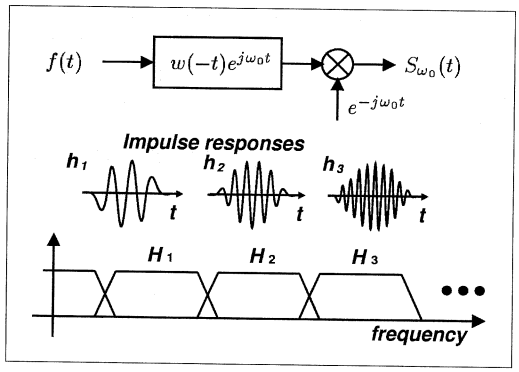

Fig. 1. Interpretation of the STFT as an infinite channel filter bank. The impulse responses of three channels of the filter bank are pictured in the time and frequency domains. The h_i's have equal support length while the H_i's have equal bandwidth. The STFT represents a fixed resolution time-frequency analysis.

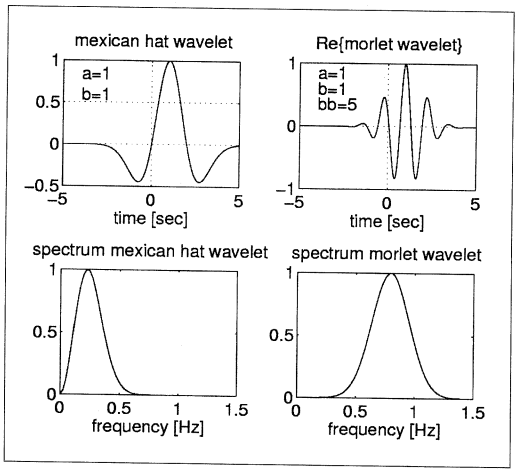

Fig. 2. Mexican-hat wavelet and Morlet wavelet in the time and frequency domain.

The parameter a is called the scale which controls the time duration of the wavelet and τ is again a translation parameter (position of the wavelet). The map spanned by the axis a and τ is called scalogram. As can be seen in (2.4) a wavelet is an oscillating function with mean value equal to zero.

In fig. 3 the functions $h_i(t) = \Psi(-t/a)$ give an example of a wavelet and show its dependence on the scale. Since (2.3) represents a scalar product it is obvious that when a trends to ∞ the CWT measures signal features on large time scales, and when a trends to zero it maps signal features on fine time scales. Thus it is able to zoom in on the signal. This property makes the CWT a useful tool for the detection of singularities.

In analogy to the STFT, the CWT's frequency resolution properties can be investigated through a filter bank view. When (2.3) is interpreted as a convolution formula then the CWT can be identified as a nonuniform infinite channel filter bank, see fig. 3. The impulse responses $h_i(t)$ are derived from dilatation of the band pass impulse response function $\Psi(-t)$ (wavelet). In contrast to the STFT, their durations depend on the scale a. Because of the dilatation property of the Fourier transform, their corresponding transfer functions $\hat{H}_i$ have the property $\Delta f_i f_i$ = constant (const. Q-analysis), where Δf_i is the bandwidth and f_i the center frequency of $\hat{H}_i$ (see Bartosch, 1996). Thus when the scale tends to ∞, the frequency resolution becomes finer. The converse is true when the scale tends to zero.

Two common types of wavelets are depicted in fig. 2. The Mexican-hat wavelet

$$\Psi(t) = (1 - 2t^2)e^{-t^2} \qquad (2.6)$$

is real valued, while the Morlet wavelet

$$\Psi(t) = (e^{-t^2/2} - \sqrt{2}e^{-b_b^2/4}e^{-t^2})e^{jb_b t} \qquad (2.7)$$

is complex. The duration and bandwidth of the Morlet wavelet can be adjusted using the modulation parameter b_b. The value of b_b gives approximately the number of cycles of the Morlet wavelet. If $b_b > \pi\sqrt{2/\ln 2} \approx 5.3364...$ the second term in the bracket in (2.7) can be neglected.

As can be seen in fig. 2 both wavelets are well localized time-frequency atoms (*). Their

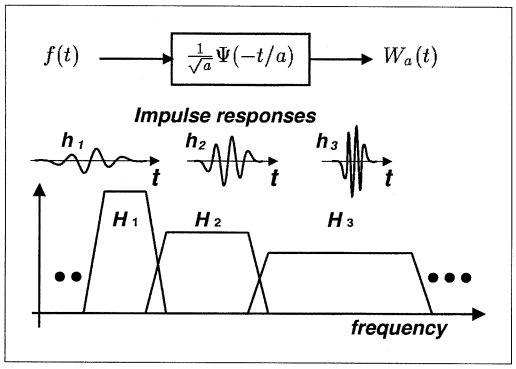

Fig. 3. Interpretation of the CWT as a non-uniform infinite channel filter bank. The impulse responses are pictured in the time and frequency domain. They are derived from dilatation of a prototype wavelet function. Therefore their support length and band width depends on the scale parameter t. The time and frequency resolution varies.

scale and center frequency are related as $f \cdot a$ = = constant. With a suitable choice of the wavelet we can therefore interpret the time-scale relationship in terms of time and frequency. In this case the constant Q property implies a logarithmic frequency axis.

A time-frequency representation is generated by mapping the tiles corresponding to the coefficients $S_{\omega,\tau}$ or $W_{a,\tau}$. Figure 6 shows the tiling of the plane for the STFT and CWT. The size of the tiles is defined by their duration T and the bandwidth B of the related transformation kernels, $h_{\omega,\tau} = w^*(t-\tau)e^{j\omega t}$ and $h_{a,\tau} = \Psi^*((t-\tau)/a)$. The tiling properties of the time-frequency plane can be summarized as follows (see Bartosch, 1996):

STFT: T = const. CWT: $T = a \cdot T_{a=1}$
B = const. $B = B_{a=1}/a$.

The time resolution for the CWT increases and the frequency resolution decreases with increasing frequency.

To compute the STFT and CWT, (2.2) and (2.3) must be discretized. See Nawab and Quatieri (1988), Vaidyanathan (1993) for discrete

(*) Well localized functions in the time and frequency domain. For details see Wickerhauser (1996).

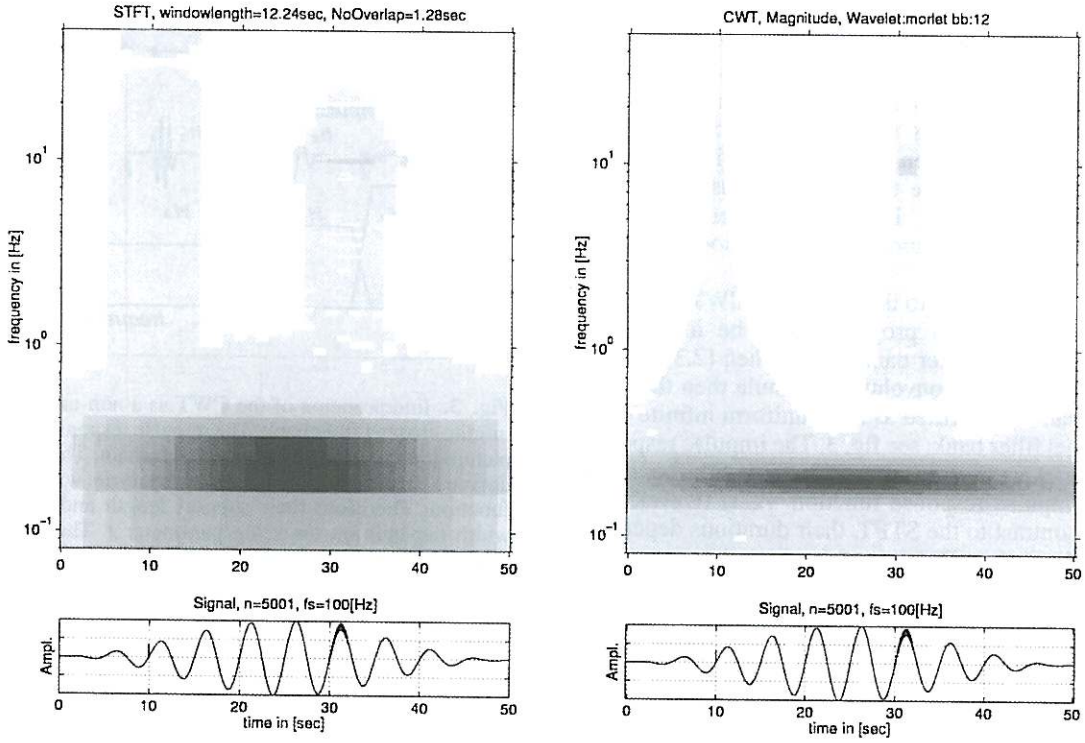

Fig. 4. STFT (left) and CWT (right) of a synthetic signal consisting of a Hanning windowed 0.2 Hz harmonic signal, a spike at 10 s and a switched ($30 < t < 33$ s) 10 Hz harmonic event. The signal is adapted to the properties of the CWT. The pulse and the beginning and end of the brief harmonic event can be resolved well using the CWT. On the other hand, the frequency of the brief harmonic event is measured more precisely using the STFT.

time STFT and Daubechies (1992), Chan (1995) for discrete time WT. Our approach to computing a time-frequency representation is based on a dense lattice ($\Delta b << T$, $\Delta f << B$) when calculating $W_{a,b}$. Therefore the coefficient map W is plotted instead of the true tiles. The result is an interpolated spectrogram.

The STFT and the CWT using a Morlet wavelet with 12 cycles ($b_b = 12$) are calculated by a synthetic signal and are pictured in fig. 4. This figure illustrates the differences between the representation of special signal features of the two transforms in the time-frequency plane. The signal is well adapted to the properties of the CWT, as it consists of a large scale (long duration) low frequency part (at 0.2 Hz) and small scale high frequency parts (pulse and switch on/off transients). In case of the STFT, the spike can hardly be recognized but the high frequency event is measured with better frequency resolution.

3. Signal analysis of selected tremor signals

Besides analyzing selected tremor signals, our intention is to emphasize differences between spectrogram analysis using STFT and CWT. For better comparison only one STFT spectrogram is computed with a rather large window length in order to include the lowest of the displayed frequency decades. An ingenious application of STFT analysis would be carried

out by calculating the STFT separately with a window length adapted to each frequency decade.

3.1. *Stromboli tremor*

Mt. Stromboli is located on the Island Stromboli in the Tyrrhenian Sea. Our analysis is based on data recorded in 1995 by J. Neuberg during an array measurement with Guralp broadband seismometers. Typically, tremor at Mt. Stromboli is continuous tremor in several dominant sub-bands with center frequencies above 1 Hz and has superimposed broadband shock events. Figure 5 gives a 250 s long example. The signal consists of two visible shock events, continuous tremor throughout the displayed time and a series of spikes at $70 < t < 100$ s.

In order to study transients during the occurrence of shocks, spectrogram analysis based on STFT (left) and CWT (right) is applied to the data. Both transforms can reveal the dominant frequency bands of the continuous tremor but the CWT gives a clearer representation of the approximate bandwidth. The first shock event contains frequencies spread out over the entire range. The STFT resolves narrow frequency bands above 3 Hz (arrows 1), while the CWT resolves the temporal behaviour far better (arrows 3). The CWT gives a blurred representation in time of the shock at lower frequencies but reveals some more complex structures along the frequency axis (arrows 2). Below $7 \cdot 10^{-2}$ Hz the window length of the STFT is not large enough to resolve three spectral lines which are correctly displayed in case of the CWT (lower three arrows 2).

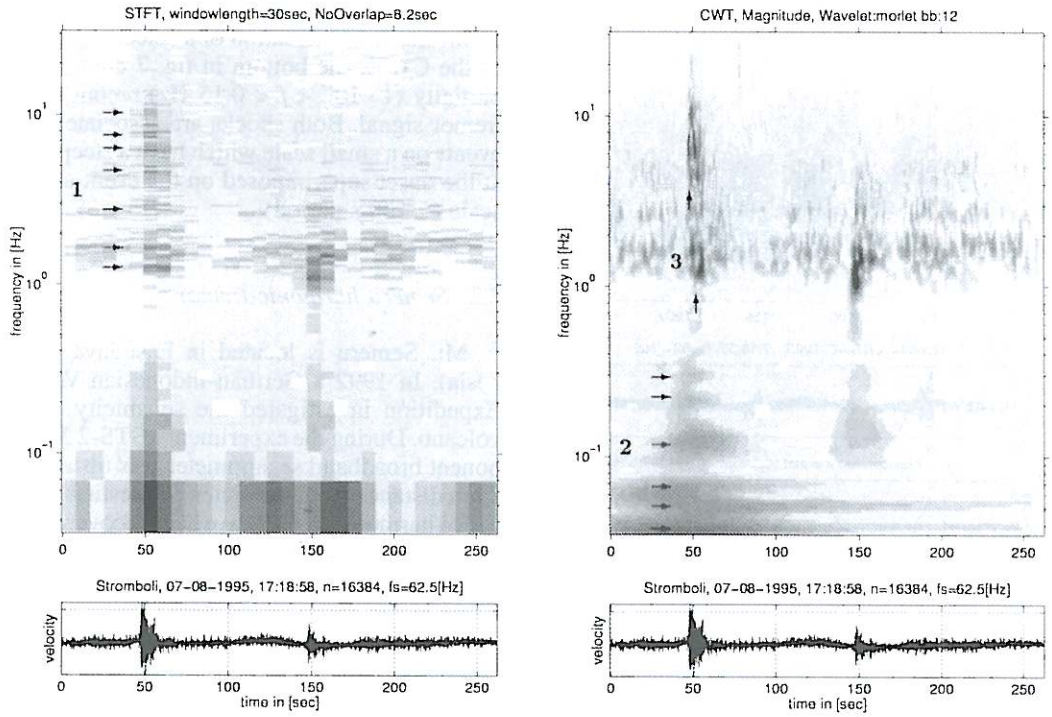

Fig. 5. STFT (left) and CWT (right) using a Morlet wavelet (12 cycles). Both maps show a different location of their maxima.

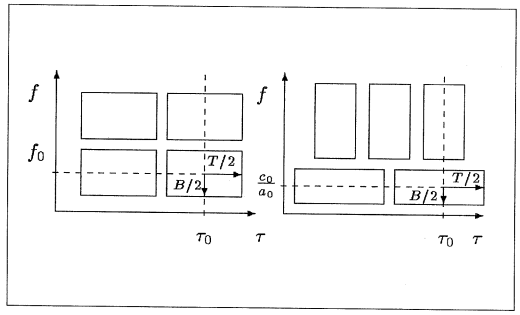

Fig. 6. Tilling of the time-frequency plane of the STFT (left) and CWT (right).

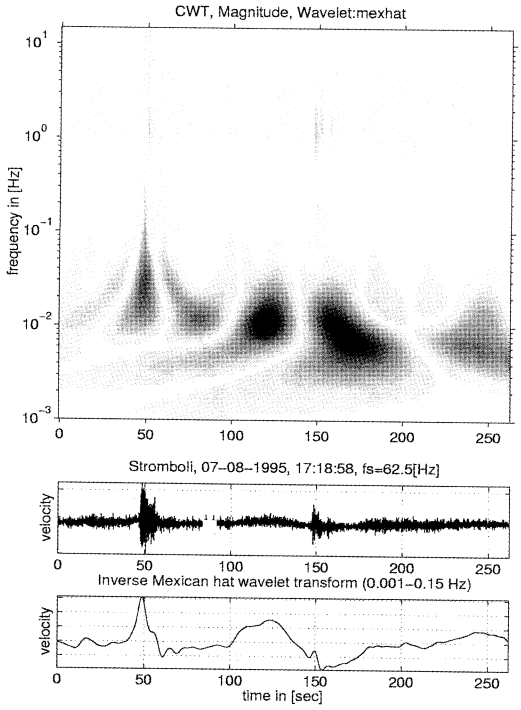

Fig. 7. CWT with a Mexican hat wavelet for studying the low frequency part of the signal. As the wavelet is real and has few cycles, the transform resolves an oscillating and well separated time pattern. The very last ray shows the reconstructed signal which belongs to the low frequency features of the signal (band pass filtered signal).

The series of spikes between $70 < t < 100$ s is resolved in case of the CWT at $f > 10$ Hz. The STFT blurs their temporal behaviour because of the long window length. In the CWT a second spike series can be recognized at $200 < t < 250$ s by comparison with first patterns.

Comparing the modulus of both spectrograms a different distribution of their maxima is found. The STFT attains its maximum in the low frequency part of the spectrogram (55 s, $5 \cdot 10^{-2}$ Hz) while the CWT displays the shock in the lowest tremor band at (150 s, 1.5 Hz) as its maximum.

A closer look at the low frequency part of the signal is displayed in fig. 7 using a CWT with a Mexican-hat wavelet. Because the wavelet has fewer cycles the spectrogram has improved time and decreased frequency resolution compared to the CWT in fig. 5. Thus, the harmonic subbands above 1 Hz cannot be separated. On the other hand, the low frequency signal content can be resolved with acceptable time resolution in a sub-band ($5 \cdot 10^{-3} < f < 5 \cdot 10^{-2}$ Hz). The related (band-pass) time signal can be extracted by inverse transformation of a selected segment of the CWT. The bottom in fig. 7 contains the partially ($1 \cdot 10^{-3} < f < 0.15$ Hz) reconstructed tremor signal. Both shocks are associated with events on a small scale which have a steep slope at the onset superimposed on the event at large scale ($\approx$ 100 s period).

3.2. *Semeru harmonic tremor*

Mt. Semeru is located in East-Java (Indonesia). In 1992 a German-Indonesian Volcano Expedition investigated the seismicity of the volcano. During the experiment a STS-2 3-component broadband seismometer was installed at 8 km distance from the crater. Interesting events called harmonic tremor have been recovered (see Hellweg *et al.*, 1994; Schlindwein *et al.*, 1994). Based on data of this station we studied the transient phenomena at the onset of such an event.

Figure 8 plots the first 80 s of a 160 s long harmonic tremor. The event consists of narrow band harmonic lines at frequencies above 0.5 Hz. Since the signal features all have similar scales, the STFT and CWT resolve approximately the same kind of information. For fig. 8

a CWT with a narrow bandwidth Morlet wavelet (large b_b) to enhance the frequency resolution was applied to the event. The fundamental and overtones can be resolved. The fundamental mode is split into two narrow lines. The spectrogram for the higher harmonics is not fine enough to determine if they follow similar behaviour. The onsets of the first three spectral lines at (0.9 Hz, 1.8 Hz, 2.7 Hz) occur at the same time while the 4th spect line jumps from $f = 3.8$ Hz to its approximate overtone frequency of 3.6 Hz at $t = 25$ s.

By inversely transforming the spectral energy of each harmonic line in a surrounding sub-band and calculating its envelope we get the

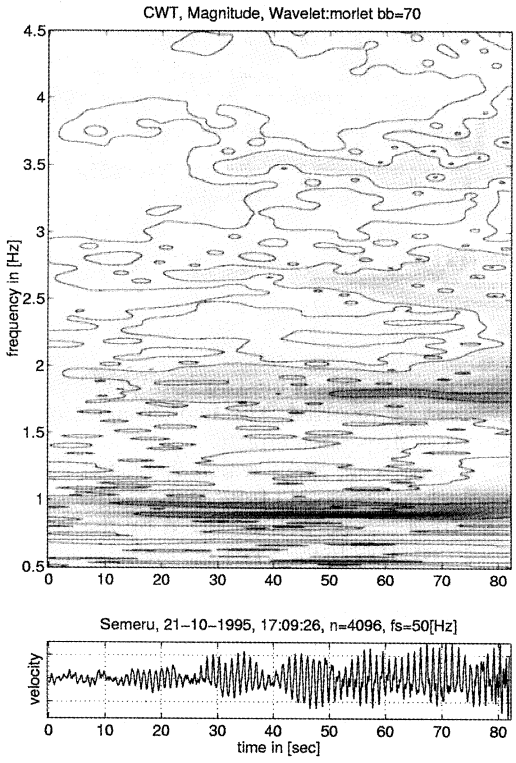

Fig. 8. CWT of a harmonic tremor event from Mt. Semeru. The fundamental and tree overtones can be recognized. The first three spectral lines have onset at the same time while the 4th line consists of a jump in frequency at 25 s.

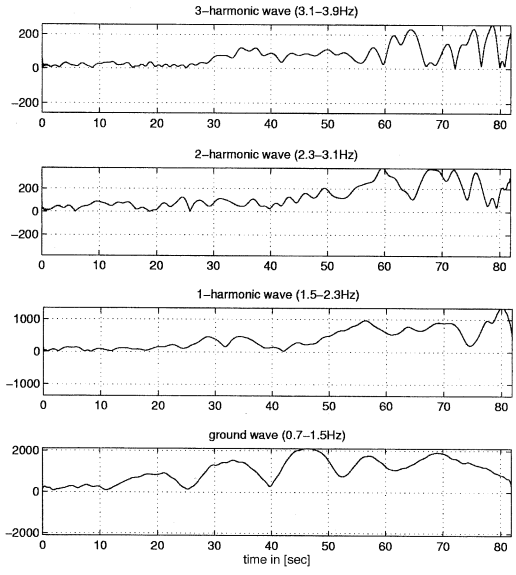

Fig. 9. Shows the envelope of the reconstructed spectral lines in a sub-band with 0.8 Hz bandwidth around the center frequencies.

amplitude of each harmonic line as a function of time (fig. 9). The splitting of the fundamental mode can be recognized as a beating phenomenon in the bottom trace. No relation between the amplitudes of the different harmonic lines can be recognized. The first and second harmonic lines seem to be delayed compared to the fundamental and third harmonic lines.

In 1995 a second expedition organized by J. Neuberg, R. Schick observed the volcanos Mt. Semeru and Mt. Bromo on East-Java and Gunung Batur on Bali. Our search for harmonic tremor events within a whole day of data from two stations located at Mt. Semeru as been unsuccessful. A source mechanism suggested in Schlindwein *et al.* (1994) might have been destroyed during large eruptions.

3.3 *Pinatubo tremor*

Figure 10 shows a 22.2 h long gravity signal recorded at Black Forest Observatory (Schiltach) with an ultra long period ET-19 seismometer.

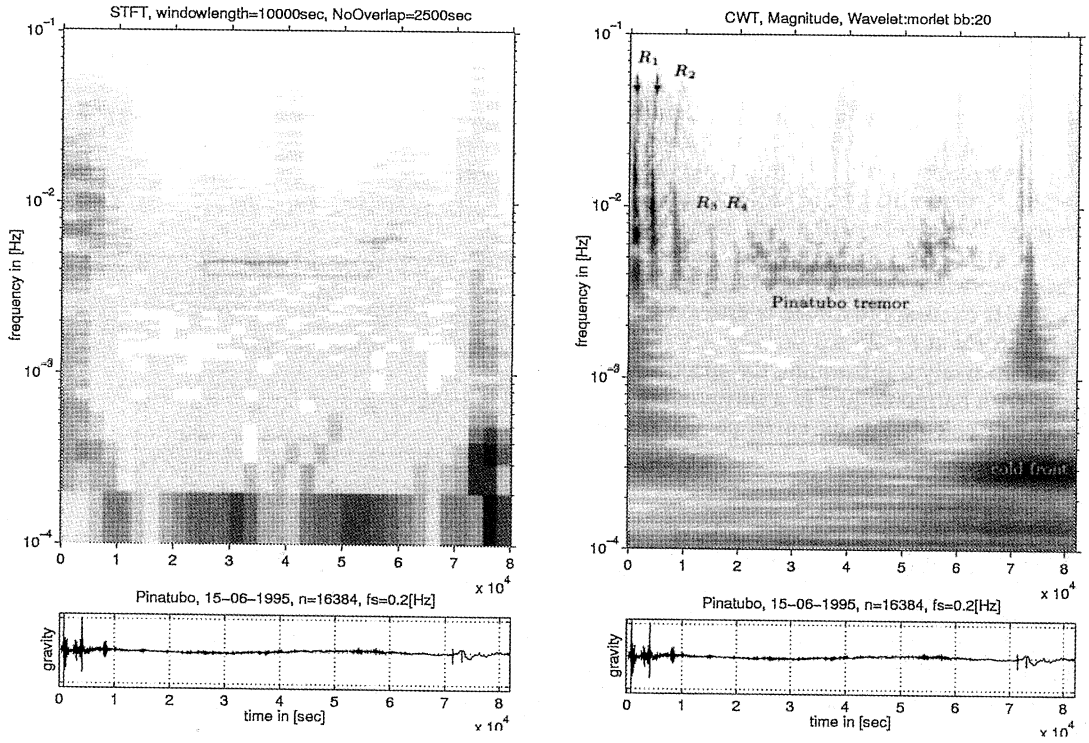

Fig. 10. STFT (left) and the CWT (right) with a Morlet wavelet (12 cycles) of 22.2 h long gravity signal recorded at BFO Schiltach.

Too narrow low frequency spectral lines are attributed to a crisis at Mt. Pinatubo volcano (see Widmer and Zürn, 1992).

In addition to the signal from the volcano, there are several seismic events on very different scales. As can be seen by comparison with the STFT in fig. 10 the CWT is a more appropriate tool for spectrogram analysis of these data.

The signal begins with several Rayleigh wave trains (R1-R4) which were generated by remote earthquakes. The time resolution is fine enough to resolve the dispersion phenomena typical for such wave trains.

The volcanic signal is represented by the two narrow harmonic lines at $3.7 \cdot 10^{-3}$ Hz and $4.4 \cdot 10^{-3}$ Hz. The spectrograms are adjusted to have approximately the same time and frequency resolution in this region. Through the zoom property of the CWT, several shock events which are superimposed on the two harmonic tremor lines can be resolved. The two strongest ones also show dispersion effects.

A large scale event which is related to an approaching local cold front at the $7 \cdot 10^4 < t < 8 \cdot 10^4$ s can be well localized by the CWT ($f \approx 2 \cdot 10^{-4}$ Hz). In the STFT the event is blurred in time.

The first shock event at $7.1 \cdot 10^{-4}$ s appears quite similar compared to two shock events around $3.9 \cdot 10^{-4}$ s and is related to a local earthquake while the second event at $7.25 \cdot 10^{-4}$ s might be caused by the seismometer itself. Its representation in the CWT spectrogram looks very similar to the CWT of the pulse in fig. 4.

A comparison between the STFT and the CWT spectrogram shows that the CWT is well adapted to the signal over the entire time- frequency plane.

4. Local coherency of Stromboli tremor

The coherency is defined as

$$C = \frac{\tilde{S}_{xy}}{\sqrt{\tilde{S}_{xx}\,\tilde{S}_{yy}}} \qquad (4.1)$$

where $\tilde{S}_{x,x}$, $\tilde{S}_{y,y}$ and $\tilde{S}_{x,y}$ are the smoothed power and cross spectra $S_{x,x}$, $S_{y,y}$, $S_{x,y}$ of the stationary processes x and y. In case of non-stationary processes this definition is inapplicable as the power and cross spectra become time-dependent. In Liu (1994) the definition of (4.1) is extended in order to be an estimate for non-stationary time series by introducing the CWT for the definitions of the power and cross spectra

$$S_{xx} = W_{a,\tau}[x(t)]W^*_{a,\tau}[x(t)]$$

$$S_{yy} = W_{a,\tau}[y(t)]W^*_{a,\tau}[y(t)]$$

$$S_{xy} = W_{a,\tau}[x(t)]W^*_{a,\tau}[y(t)]$$

as time-depended estimators. Translating the scale into a frequency parameter f and using a logarithmic mapping for f gives a constant resolution along the frequency axis. Smoothing along the frequency axis can therefore be performed by convolution with a constant-length window function. As we implemented our CWT with a constant grid for the translation parameter b to get rectangular maps $W_{a,\tau}$, we must adapt our window length for smoothing along the time axis which depends on the scale. The window length is then $W_l = W_{l,\mathrm{init}}/f$. Each row of the map C has to be convolved with a window of length w_l. The solid line in fig. 11 shows $w_l(f)$ in second as a function of frequency.

Figure 11 plots recordings of time series of tremor with superimposed shock events for two stations FOS and OBS located near the craters of Mt. Stromboli along with their local coherency. In the frequency band above 0.3 Hz the coherency pattern is similar for all shocks. Also the coherency around 0.2 Hz (sea microseismic) breaks down during the occurrence of the shocks. For a more detailed interpretation of local coherency applied on data from Mt. Stromboli (see Wassermann, 1997).

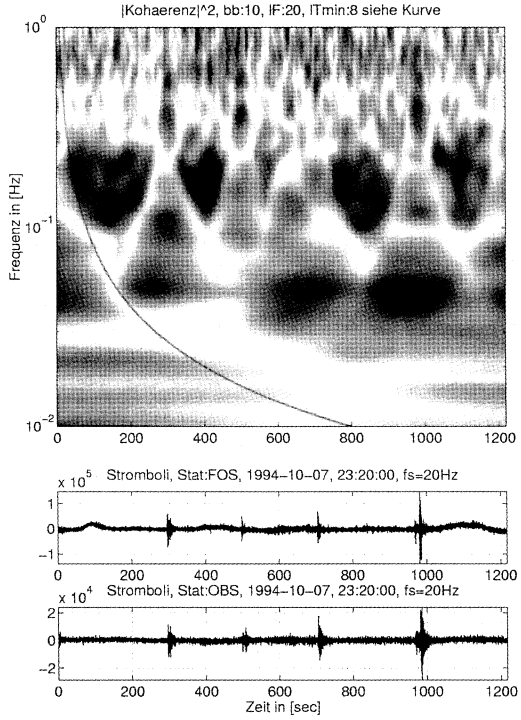

Fig. 11. Local cohereny of two seismic signals recorded at FOS and OBS station at Mt. Stromboli near the craters. All shock events consist of similar correlation pattern especially at frequencies above 1 Hz while the correlation of the sea microseismic (0.2 Hz) breaks down during the occurrence of a shock. The solid line indicates the duration of the smoothing window.

5. Conclusions

The spectral analysis of three different tremor signals shows that the advantages of the CWT compared to STFT depend highly on the properties of the signal itself. The CWT proved to be useful for analyzing signals which consist of information in very different time scales, *e.g.*, Pinatubo tremor. The CWT can provide spectrograms presenting the spectral information over several frequency decades resulting in an improved insight into the nature of broadband signals.

Using an array of stations, the WT can be applied to the determination of the local spatial coherency as a function of time and scale.

Acknowledgements

The authors wish to thank J. Neuberg (Department of Earth Science, University of Leeds, U.K.), W. Zürn (BFO Schiltach, Germany) and J. Wassermann (Department of Geophysics, University of Munich, Germany) for placing data at our disposal and for their advice and help in many discussions. We thank (M. Hellweg, University Stuttgart, Germany) for previewing this text and for many suggestions.

REFERENCES

BARTOSCH, T. (1996): Arbeitsbericht: August 1994-Januar 1996, *Technical Report*, Lehrstuhl für Nachrichtentechnik, Universität Erlangen-Nürnberg.

CHAN, Y. (1995): *Wavelet Basics* (Kluwer Academic Publishers, Boston), 23-49.

DAUBECHIES, I. (1992): *Ten Lectures on Wavelets,* Society for Industrial and Applied Mathematics, Philadelphia.

HELLWEG, M., D. SEIDL, S.B. KIRBANI and W. BRÜSTLE (1994): Team investigates activity at Mt. Semeru, Java, Volcano, *Eos, Trans., Am, Geophys. Un.*, **75** (28), 313-317.

LIU, P. (1994): Wavelet spectrum analysis and ocean waves, in *Wavelets in Geophysics*, edited by E. FOUFOULA-GEORGIOU and P. KUMAR (Academic Press Inc., London), 151-167.

NAWAB, S. and T. QUATIERI (1988): Short-time Fourier transform, in *Advanced Topics in Signal Processing*, edited by J.S. LIM and A.V. OPPENHEIM (Prentice Hall., New Jersey), 289 f.

SCHLINDWEIN, V., J. WASSERMANN and F. SCHERBAUM (1994): Spectral analysis of harmonic tremor signals, *Geophys. Res. Lett.*, **22** (13), 1685-1688.

VAIDYANATHAN, P. (1993): *Multirate Systems and Filter Banks* (Prentice Hall, New Jersey), 463 f.

WASSERMANN, J. (1997): Untersuchung seismischer Signale vulkanischen Ursprungs anhand von Breitband – Arrayregistrierungen an den Vulkanen Ätna und Stromboli, *Ph.D. Thesis*, Institut für Geophysik, Universität Stuttgart.

WICKERHAUSER, M. (1996): *Adaptive Wavelet-Analyse* (Vieweg Verlag, Braunschweig/Wiesbaden), p. 9.

WIDMER, R. and W. ZÜRN (1992): Bichromatic exitation of long-period rayleigh and air waves by the mount Pinatubo and El Chichon volcanic eruptions, *Geophys. Res. Lett.*, **19** (8), 765-768.